Available online at www.sciencedirect.com

ScienceDirect

Ceramics International 40 (2014) 9715–9721

CERAMICS INTERNATIONAL

www.elsevier.com/locate/ceramint

The effect of a constraint on the sintering and stress development in alumina thick films

Mark Tillman[a], Julie A. Yeomans[a,*], Robert A. Dorey[b]

[a]Department of Mechanical Engineering Sciences,Faculty of Engineering and Physical Sciences, University of Surrey, Guildford GU2 7XH, UK
[b]School of Applied Science, Cranfield University, College Road, Cranfield MK43 0AL, UK

Received 19 December 2013; received in revised form 11 February 2014; accepted 12 February 2014
Available online 20 February 2014

Abstract

The microstructural and stress evolution of thick (25 μm) alumina films on dense alumina substrates sintered at temperatures from 1300 °C to 1600 °C has been investigated. In this study the constraint on sintering was monitored in the absence of significant differences in thermal expansion between the film and the substrate. For comparison purposes unconstrained alumina pellets sintered at 1300 °C–1600 °C were also examined. Overall, the constrained alumina densified less than the free alumina, as expected, although at intermediate temperatures densification rates were comparable. Sintering in the direction perpendicular to the substrate was enhanced with respect to that parallel to the substrate as a means of stress relaxation. Using fluorescence spectroscopy the residual stresses of the films parallel to the substrates were measured; residual tensile stresses as high as 450 ± 40 MPa were exhibited by the films. The considerable stress development resulted in cracking and delamination of the film from the substrate, subsequently film constraint was reduced and densification was not impeded.

Keywords: A. Sintering; B. Microstructure; D. Alumina; Stress

1. Introduction

Free sintering is a well-known method for the manufacture of monolithic ceramic bodies from a porous powder compact. However, for some applications a ceramic is integrated and co-sintered with a number of other ceramic or non-ceramic materials. Often one or more of the ceramic components is in the form of a porous film of powder on a denser substrate such that non-matched sintering rates of the integrated materials are exhibited, and sintering of the powder compact (film) becomes constrained [1–3]. The substrate material is considered to be a rigid inclusion if it does not deform when the integrated green ceramic shrinks during drying and sintering [4]. As a consequence the shrinkage of the ceramic during sintering in the directions parallel to the substrate is fully constrained and internal tensile stresses develop as a result, but the direction perpendicular to the substrate is considered free from the constraint [5,6]. The effect of the constraint on film shrinkage was examined by Garino and Bowen [7] by monitoring the shrinkage of fully constrained and free zirconium oxide films using laser dilatometry and electron microscopy. The constrained films exhibited much slower rates of volumetric shrinkage with final shrinkages of 14% compared with free shrinkages of 24%. Restrictions on shrinkage in constrained bodies were originally explained by Bordia and Raj [1] to occur due to the grain necks in the directions parallel to the rigid inclusion being under tensile stresses, leading to a reduction in the flow of matter and the mobility of the grain boundaries in these directions. In more recent computer simulations the viscous drag effect of the substrate on the particle contact interactions has been studied [8]. The viscous drag, which is more pronounced closer to the substrate, results in the loss of contact between certain particles in the sintering ceramic as the substrate drag forces resist normal densifying sintering forces. This contact disruption has two results; firstly pores that are directed perpendicular to the

*Corresponding author. Tel.: +01483 689613.
E-mail address: j.yeomans@surrey.ac.uk (J.A. Yeomans).

http://dx.doi.org/10.1016/j.ceramint.2014.02.054

substrate open, and secondly there is a reduction on the constraint of the particles due to some contacts being absent resulting in contact growth with neighbouring particles where the contact still remains intact. These sintering mechanisms result in isotropic green microstructures becoming anisotropic during sintering.

As a result of the shrinkage mismatches between the sintering ceramic and the rigid substrate, tensile stresses develop in the sintering ceramic. These stresses can be transient if relieved by stress relaxation mechanisms such as creep, cracking or delamination, but usually residual stress in constrained ceramics are identified [9]. Stress development also arises due to thermal expansion coefficient mismatches between the integrated materials. The Stoney bending method and the X-ray diffraction tilting method have been used to determine the average residual stress in thin ceramic films [10–12]. There has also been successful non-destructive evaluations of localised residual stresses in alumina ceramics using the Raman and fluorescence spectroscopic methods [9,13,14]. Unstressed alumina exhibits a characteristic peak in Raman intensity at a wavenumber of 417 cm^{-1} when excited by a laser [13,15]. Unstressed alumina also exhibits the characteristic R1 and R2 fluorescence peaks of ruby at 14,402 cm^{-1} and 14,432 cm^{-1}, respectively, when excited. The R1 and R2 peaks originate from the photon emission of photostimulated Cr^{3+} impurities that commonly substitute for Al^{3+} ions in alumina [16]. The Raman, R1 and R2 peaks shift to a lower wavenumber when alumina is under a compressive stress and shift to a higher wavenumber when under a tensile stress [16,17], with the magnitude of the residual stress determined from the peak shifts. However, there is a difficulty in calculating stress from the R1 peak shift [18], and so it has not been used in stress determination by many authors [15,19]. There is a tensor relationship between the shift in the R2 peak in units of cm^{-1}, $\Delta\upsilon_{R2}$, and the magnitude of the stress in GPa that the alumina ceramic is under. This tensor relationship simplifies to a hydrostatic stress component, σ_h, as defined in the following equation: [15,20].

$$\sigma_h = \Delta\upsilon_{R2}/7.61 \quad (1)$$

In these stress determining methods the volume of material analysed is dictated by the size of the laser spot, which is usually only a few micrometres in diameter. It is also dependent on the depth of penetration of the laser through the sample which is a function of porosity and grain size of the target material, but in alumina it has been reported to be between 10 and 25 μm for fluorescence spectroscopy and as low as 2 μm for Raman spectroscopy [13,20,21].

The aim of this paper is to compare the microstructural and stress evolution of free and constrained sintered alumina. This was done by processing freely sintered alumina pellets and comparing the analysis of densification, grain growth and stress development with that of sintered screen-printed 25 μm thick alumina films integrated with dense alumina substrates. In this way the effect of constrained sintering and sintering stresses on alumina ceramics is monitored in the absence of significant differences in thermal expansion.

2. Experimental procedure

Alumina ink was prepared by mixing 56 g of alumina powder with a 0.7 μm mean particle size and 18.7 g of polyethylene glycol 6000 binder in a round bottomed flask. 16.4 ml of ethylene glycol (anhydrous 99.8%), 7.1 ml of de-ionised water and 1.3 ml of Surfynol dispersant (CT-324) were added to this. This solution was mixed for 2 h in an ultrasonic bath at 40 °C, before being left to cool. The ink was deposited onto 1 mm thick alumina substrates using a DEK 245 screen-printer with a screen thickness of 110 μm, mesh screen of 65 apertures/cm and a squeegee speed of 4 cm s^{-1}. Two layers were deposited with drying at 150 °C for 1 min after each deposition to produce a 25 μm thick film. The films were then heated in a furnace at a heating rate of 2 °C/min to a hold temperature of 600 °C for 30 min in order to remove all solvents and binder. Alumina pellets were prepared from the same alumina powder as used in the ink without any further additives, and pressed at 6 metric tonnes for 5 min using a Specac pellet press (Slough, UK). The resultant pellets were 13 mm in diameter and 2.6 mm thick. The films and pellets were heated in a furnace at 2 °C/min heating rate and sintered at isothermal temperatures between 1300 °C and 1600 °C for a hold time of 2 h.

The residual stresses of the pellets and films were determined using a Varian Cary Eclipse fluorescence spectrometer and a Renishaw MicroRaman spectrometer. The cross sections of the films were too small to analyse accurately by using these processes, so the top surfaces of the pellets and films were exposed to the lasers of the two systems. With this there was a degree of depth penetration using these systems [13,20,21]. In the fluorescence spectroscopy process a 5 mm laser spot at a wavelength of 346 nm was directed towards the samples to determine the R2 peaks. Analysis was conducted across 4 different samples at 3 different positions per sample and values were averaged for each data point. In the Raman spectroscopy process a 2 μm laser spot at a wavelength of 782 nm was directed towards the samples across 4 different samples at 5 different positions per sample and the data were averaged for each data point.

The processed films and pellets were then cut to expose the cross sections followed by mounting in epoxy in preparation for scanning electron microscopy (SEM) imaging. The samples were progressively polished starting with a 60 μm diamond pad and finished with a 1 μm diamond grit size (Stuers, Copenhagen, Denmark). The samples were then coated with ~3 nm of evaporated gold and imaged using a Hitachi S-3200N scanning electron microscope.

3. Results

3.1. Microstructural evolution

The relative density and grain sizes of the green and sintered films and pellets were determined from micrographs (Fig. 1) using the linear intercept technique [22] across combined distances of at least 1000 μm and 800 intercepts. In these

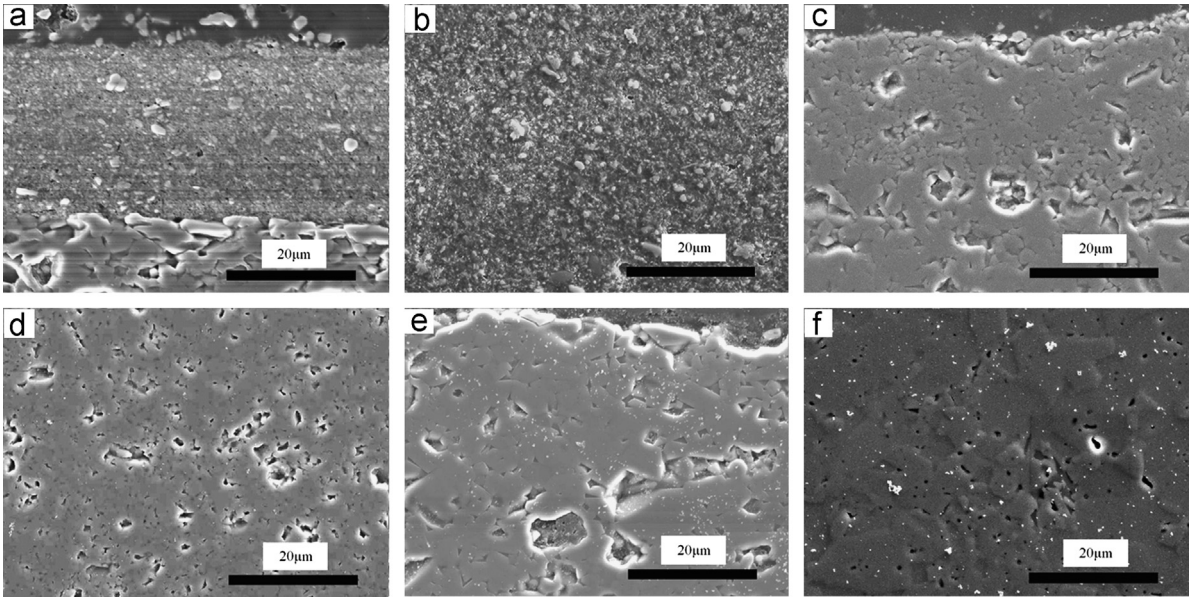

Fig. 1. SEM micrographs of an a) green (not sintered) film, b) green (not sintered) pellet, c) film sintered at 1500 °C, d) pellet sintered at 1500 °C, e) film sintered at 1600 °C, and f) pellet sintered at 1600 °C.

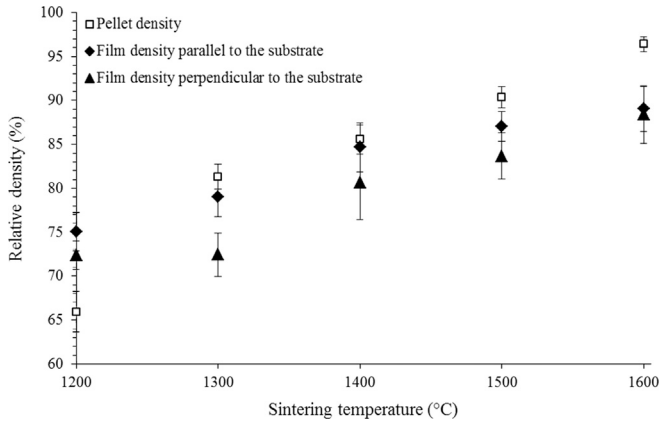

Fig. 2. Relative density of pellets and films as a function of sintering temperature.

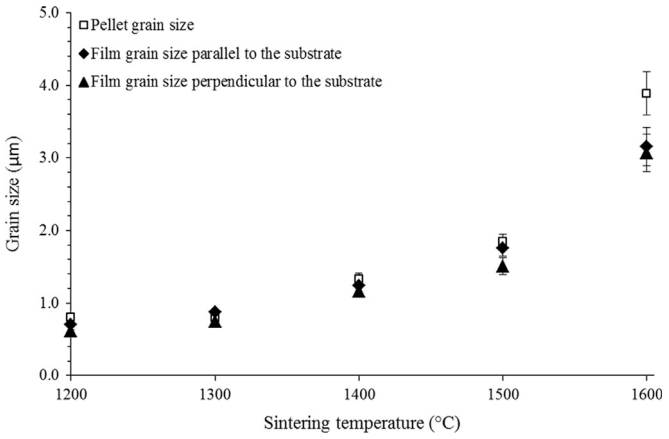

Fig. 3. Grain size of pellets and films as a function of sintering temperature.

images the less dense film can be seen to be integrated with the dense substrate, although the interface becomes increasingly difficult to identify for the films sintered at higher temperatures. The density and grain size both increase with increasing sintering temperature. The relative density as a function of sintering temperature is displayed in Fig. 2. The starting density of the pellets was ~66%, and there was a linear trend of the density increasing with increase in the isothermal temperature, resulting in a final density of 96% for the pellets sintered at 1600 °C. In comparison, the starting density of the films was higher with values of 72% and 75% perpendicular and parallel to the substrate, respectively, potentially due to the ability to more easily rearrange the particles in the fluid screen printing ink system. After sintering at 1300 °C the density of the film parallel to the substrate is comparable to that of the pellets, with the pellets having undergone significant densification. No densification was observed perpendicular to the substrate. Such behaviour could be accounted for by preferential neck breakage in the direction perpendicular to the substrate compounded by the slight anisotropy in film density in the two directions following printing. When sintered at 1400 °C and above, the films initially exhibit greater increases in density compared to the pellets before showing smaller incremental changes in density following sintering at 1500 °C and 1600 °C, with the density parallel to the substrate being affected to a greater degree. After sintering at 1600 °C the films exhibit a comparable density (88%) both parallel and perpendicular to the substrate.

The grain sizes as a function of sintering temperature are shown in Fig. 3. The starting grain sizes are 0.6–0.8 μm and it can be seen that the sizes of the grains in the pellets and films slowly increase in all directions at similar rates up to 1500 °C. After sintering at 1600 °C the grains in the pellets have greatly increased in size, with a final average grain size of 3.9 μm. The average sizes of the grains in the films also greatly increase with a final size of 3.1 μm. Similar grain sizes are seen in all directions in the films, so it is evident that uniform grain

growth occurred which has previously been seen with constrained sintering [23]. Grain size as a function of the relative density for each sample is shown in Fig. 4 and highlights the reliance of grain growth on particle contact within the ceramic matrix. For a given density the average grain size in the films is larger than that in the pellets. Such grain growth at the expense of densification is thought to be a consequence of the reduction in densification rates caused by a decrease in the densification activation energy due to constrained sintering stresses [24]. Such stresses do not affect grain growth rates in the same manner and mean that there is more time for grain growth to take place when high densities are desired.

In the microstructural analysis of the films there were also cracks and delamination as shown in (Fig. 5) which are likely to have had an effect on the sintering of the films. The green film was uniform in thickness with no cracks observable. After sintering at 1300 °C there were a number of minor cracks observed; in Fig. 5a there was a crack close to the interface. Sintering at 1400 °C and 1500 °C resulted in an increase in the number and size of cracks (Fig. 5b and c), suggesting that the stress increased as the sintering temperature increased. These large cracks usually span the entire thickness of the film, resulting in regions where there was no film–substrate contact. While cracks were also observed in the films sintered at 1600 °C, the edges of the films had also completely delaminated from the substrate (Fig. 5d). The film–substrate contact area was determined from the micrographs and is displayed in Table 1. The film-substrate area progressively decreases as the sintering temperature increases from 1300 °C to 1500 °C, yet does not decrease further when after sintering at 1600 °C, indicating an end to the relaxation mechanism or the fact that sintering stresses did not increase further.

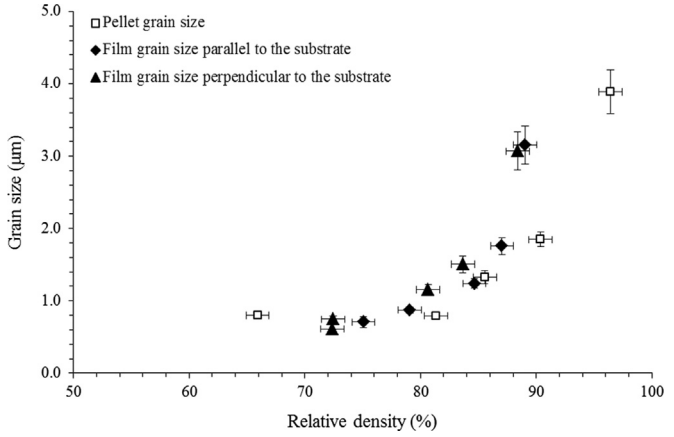

Fig. 4. Grain size of pellets and films as a function of the relative density of the pellets and films.

3.2. Stress evolution

It is apparent from the cracks and delamination present in the films that increases in stress and subsequent stress relief occurred during sintering. The residual stress in the films was monitored using the Raman spectroscopy, with the averaged

Table 1
Film-substrate contact area, estimated from micrographs, as a function of sintering temperature.

Sintering temperature (°C)	Film-substrate contact area (%)	± error
1300	98	2
1400	93	3
1500	88	5
1600	88	3

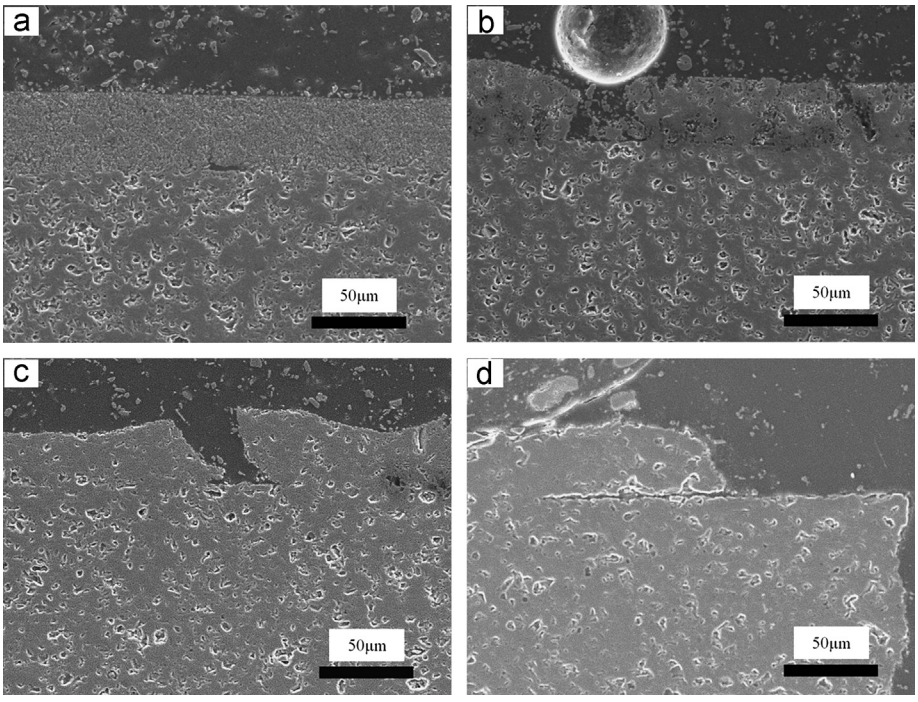

Fig. 5. SEM micrographs of films sintered at a) 1400 °C, b) 1500 °C, and c) 1600 °C.

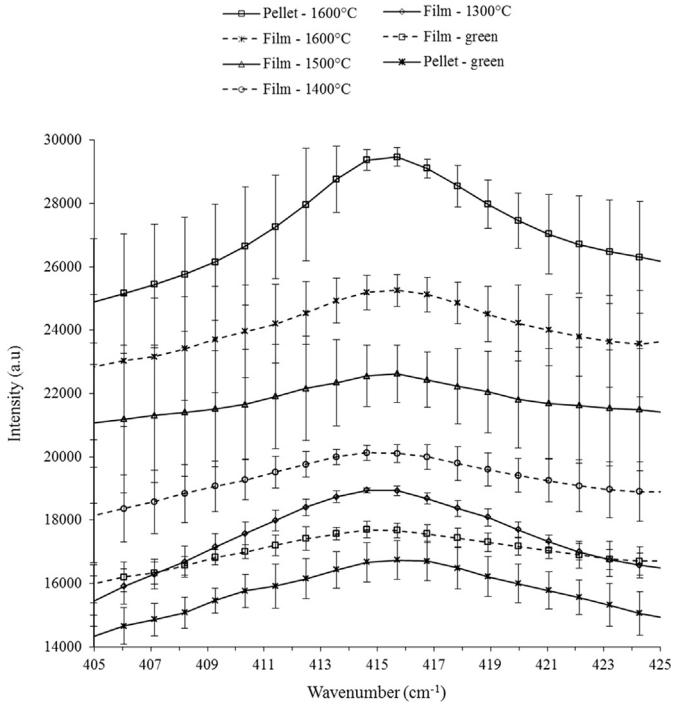

Fig. 6. Raman spectrum of the green pellets, green films and films sintered at 1300 °C, 1400 °C, 1500 °C and 1600 °C, respectively.

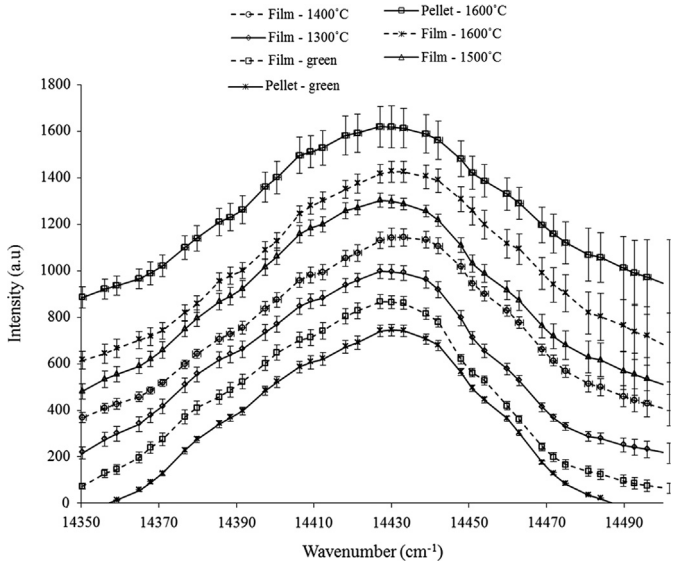

Fig. 7. R2 florescence spectrum obtained from the green pellets, green films and films sintered at 1300 °C, 1400 °C, 1500 °C and 1600 °C, respectively.

spectra displayed in Fig. 6. There are relatively high errors, possibly due to differences in the reflection of the laser on the surface of the ceramics, which reduce at the peak of each spectrum. The green pellets and green films exhibit identical peak positions at 415.1 cm^{-1}, with no change after sintering at 1300 °C and 1400 °C, suggesting that there was no residual stress present. After sintering at 1500 °C and 1600 °C the peak position moves to 415.7 cm^{-1}, which indicates that these films were under a small residual tensile stress. The residual stress was also monitored using the R2 fluorescence spectra, displayed in Fig. 7. The errors are much lower than seen with the Raman spectra yet more broadened due to the larger surface area of the ceramic examined. The peak positions exhibited by the green pellet, green film and film sintered at 1300 °C are comparable. This is followed by a shift to higher wave number for films sintered at 1400 °C and 1600 °C which occurs as a consequence of residual tensile stresses. The decrease in wavenumber for peak position of the sample sintered at 1500 °C indicates a slight compressive stress. The mean R2 peak positions and the calculated residual stresses are displayed in Table 2. The wavenumber of the green pellet is high in comparison with the sintered pellet and films; this is likely to be due to residual tensile stresses near the surface of the pellet as a consequence of elastic spring-back following pressing of the powder. For this reason the peak position exhibited by the green film has been used as the stress free state, with the peak shift from this position used to determine residual stresses using Eq. 1. The films sintered at 1300 °C exhibit a small residual tensile stress which greatly increases to 450 ± 40 MPa after sintering at 1400 °C. A similar value (350 ± 90 MPa) is observed after sintering at 1600 °C with the films sintered at 1500 °C exhibiting an apparent residual compressive stress.

Tensile stresses have been confirmed to arise in the constrained sintered films, but the trends observed using the Raman and fluorescence spectroscopic processes differ. This can be explained by the difference in depth of penetration of the lasers in the two methods. In the fluorescence spectroscopic process the depth of penetration in alumina has been reported to be at least 10 μm and may increase up to 25 μm when the sample is of low density and has small grains [13,20,21]. It is likely, therefore, that a significant depth of the films was examined with the depth of penetration of the laser reducing as the films were sintered at higher temperatures. Conversely, in the Raman spectroscopic process only the top surface of the films was analysed as the depth of penetration with alumina may be as low as 2 μm [13]. This would lead to a greater averaging, and peak broadening, when using fluorescence spectroscopy. With a 5 mm spot size and greater depth of penetration, both cracked and un-cracked materials were examined such that regions of high and low stress were sampled. With Raman spectroscopy there is a much smaller sampling volume, so unless a crack is directly targeted the apparent residual stress would be more representative of the surface layer.

4. Discussions

Usually, in constrained films it is considered that the densifying matter flow in the direction perpendicular to the substrate is free from constraint and densification in this direction may even accelerate as compared with freely sintered films; conversely densification in the directions parallel to the substrate is considered to be fully constrained due to constrained neck growth, tensile stress effects and substrate viscous drag, so microstructural heterogeneities develop [1,5,6,8]. In this study, while considerable densification occurred both parallel and perpendicular to the substrate in

Table 2
Mean R2 fluorescence peak positions and residual stress of the green pellets and pellets sintered at 1600 °C and the green films and films sintered at 1300 °C, 1400 °C, 1500 °C and 1600 °C, respectively.

Sintering temperature (°C)	Mean peak position (cm^{-1})	± error	Mean residual tensile stress (MPa)	± error
Pellet – green	14,431	0.8		
Pellet –1600	14,427	1.7		
Film – green	14,428	1.7	0	0
Film – 1300	14,429	1.2	80	60
Film – 1400	14,432	1.4	450	40
Film – 1500	14,428	1.0	-20	100
Film – 1600	14,431	1.0	350	90

the films, there was a slightly higher degree of densification perpendicular to the substrate. Despite this the presence of significant densification in both directions is consistent with relief of constraint of the substrate, possibly due to non-rigidity, sintering of the substrate or stress relief mechanism operating within the film. Upon inspection there was no curvature of the substrate, and the relative density of the substrate, as determined from the micrographs, was the same after each processing temperature at $87 \pm 2\%$ indicating that constraint relief must originate from within the film itself. Here the observed cracking and delamination of the film could locally relieve the constraint while matter rearrangement, manifesting in differences in sintering rates parallel and perpendicular to the substrate, would result in large scale stress relaxation.

Cracking and delamination occur as a result of the tensile strength of the sintering ceramic film being surpassed. Cai et al. [25] examined the cracking that developed as a result of tensile sintering stresses, in-plane with the bilayer interface, in the faster sintering zirconia layers of alumina-zirconia bilayers. Clean, brittle cracks developed perpendicular to the direction of the stress with cracking also occurring through the linkage of pores due to thermal expansion mismatches. This has not been seen in this study due to absence of any significant thermal expansion mismatches between the substrate and the film. Furthermore, cracking in close proximity and parallel to the interface was seen. Such delamination at the edges of ceramic films has been attributed to the preferred densification of constrained films perpendicular to the substrate [26].

From the results obtained, a sequence of events that occurred during the sintering of the alumina films is now postulated. Upon sintering the uniform green alumina films at 1300 °C, there was a low degree of densification, with the majority of sintering occurring perpendicular to the substrate. The limited densification that occurred parallel to the substrate was opposed by the rigid substrate and resulted in a small residual tensile stress. As the sintering temperature was increased the density increased in all the films in all directions, with the rate being nearly as high as that exhibited by the freely sintered pellets. As a result of the densification parallel to the substrate being opposed by the rigidity of the substrate a high tensile stress (350–450 MPa) was developed. This led to cracking and delamination in areas where the stress exceeded the local material or interface strengths, such that for the material sintered at 1500 °C, a small compressive residual stress (or possibly a very small tensile stress, given the uncertainty in the measurement) was observed when using fluorescence spectroscopy, which has a larger sampling volume and hence the possibility of accessing a broader range of stress states throughout the thickness of the film/substrate system. On further heating to 1600 °C, it seems that the cycle of stress accumulation starts over again.

5. Conclusions

In this study the development of density, grain size and stress in alumina when under constrained and free sintering was evaluated, using a combination of microscopy and spectroscopy techniques. The density and grain size were shown to increase, less in the alumina films than in the freely sintered pellets, for a given sintering condition. When films and pellets of comparable density are considered, grain growth is enhanced in the films, possibly as a route to stress relief. The presence of sintering tensile stresses led to sintering parallel to the substrate slowing at higher temperature. Despite this, there was a significant densification of the constrained films (particularly at intermediate temperatures), with a rate of density increase almost as high as seen during free sintering. Although a significant residual tensile stress was observed to be present in the films sintered at 1400 °C and 1600 °C; no appreciable stress was recorded for the films sintered at 1500 °C, suggesting a cyclic process in which stress formation, which hinders densification, is followed by stress relief, via cracking and delamination, which allows local densification to occur.

Acknowledgements

The authors gratefully acknowledge the support provided by the Engineering and Physical Sciences Research Council (Grant reference EP/F041853/1).

References

[1] R.K. Bordia, G.W. Scherer, On constrained sintering-III: Rigid inclusions., Acta Metall. 36 (9) (1988) 2411–2416.
[2] R.K. Bordia, A. Jagota, Crack growth and damage in constrained sintering films, J. Am. Ceram. Soc. 76 (10) (1993) 2475–2485.

[3] M.N. Rahaman, in: Ceramic Processing and Sintering, 2nd ed., Marcel Dekker, Inc., New York, 1995.
[4] R.K. Bordia, R. Raj, Sintering behaviour of ceramic films constrained by a rigid substrate, J. Am. Ceram. Soc. 68 (6) (1985) 287–292.
[5] A. Cipitria, I.O. Golosnoy, T.W. Clyne, A sintering model for plasma-sprayed zirconia thermal barrier coatings. Part II: coatings bonded to a rigid substrate, Acta Mater. 57 (4) (2009) 993–1003.
[6] R.A. Dorey, R.W. Whatmore, Electroceramic thick film fabrication for MEMS, J. Electroceram. 12 (1–2) (2004) 19–32.
[7] T.J. Garino, H.K. Bowen, Deposition and sintering of particle films on a rigid substrate, J. Am. Ceram. Soc. 70 (11) (1987) c. 315–c. 317.
[8] C.L. Martin, R.K. Bordia, The effect of a substrate on the sintering of constrained films, Acta Mater. 57 (2) (2009) 549–558.
[9] G. De Portu, L. Micele, Y. Sekiguchi, G. Pezzotti, Measurement of residual stress distributions in Al2O 3/3Y-TZP multilayered composites by fluorescence and Raman microprobe piezo-spectroscopy, Acta Mater. 53 (5) (2005) 1511–1520.
[10] S. Corkovic, R.W. Whatmore, Q. Zhang, Development of residual stress in sol–gel derived Pb (Zr,Ti) O3 films: an experimental study, J. Appl. Phys. 103 (2008) 8.
[11] T. Ohno, B. Malić, H. Fukazawa, N. Wakiya, H. Suzuki, T. Matsuda, et al., Origin of compressive residual stress in alkoxide derived $PbTiO_3$ thin film on Si wafer, Jpn. J. Appl. Phys. 47 (9 PART 2) (2008) 7514–7518.
[12] G.G. Stoney, The tension of metallic films deposited by electrolysis, Proc. R. Soc. Lond. 82 (1909) 172–175.
[13] S. Ohtsuka, W. Zhu, S. Tochino, Y. Sekiguchi, G. Pezzotti, In-depth analysis of residual stress in an alumina coating on silicon nitride substrate using confocal Raman piezo-spectroscopy, Acta Mater. 55 (4) (2007) 1129–1135.
[14] H.Z. Wu, S.G. Roberts, B. Derby, Residual stress distributions around indentations and scratches in polycrystalline Al_2O_3 and Al_2O_3/SiC nanocomposites measured using fluorescence probes, Acta Mater. 56 (1) (2008) 140–149.
[15] J.A. Pardo, R.I. Merino, V.M. Orera, J.I. Peña, C. González, J.Y. Pastor, et al., Piezospectroscopic study of residual stresses in Al_2O_3-ZrO_2 directionally solidified eutectics, J. Am. Ceram. Soc. 83 (11) (2000) 2745–2752.
[16] J. He, D.R. Clarke, Determination of fibre strength distributions from bundle tests using optical luminescence spectroscopy, Proc. R. Soc. A 453 (1964) (1997) 1881–1901.
[17] X. Wang, A. Atkinson, Piezo-spectroscopic mapping of the thermally grown oxide in thermal barrier coatings, Mater. Sci. Eng. A 465 (1–2) (2007) 49–58.
[18] Y.M. Gupta, X.A. Shen, Potential use of the ruby R2 line shift for static high-pressure calibration, Appl. Phys. Lett. 58 (6) (1991) 583–585.
[19] X. Zhao, P. Xiao, Focus effect of photoluminescence piezospectroscopy and its influence on the stress measurement of thermally grown oxide in thermal barrier coatings, Scr. Mater. 57 (8) (2007) 683–686.
[20] X. Wang, P. Xiao, Residual stresses and constrained sintering of YSZ/Al_2O_3 composite coatings, Acta Mater. 52 (9) (2004) 2591–2603.
[21] S. Guo, R.I. Todd, Confocal fluorescence microscopy in alumina-based ceramics: where does the signal come from?, J Eur. Ceram. Soc. 30 (3) (2010) 641–648.
[22] J.C. Wurst, J.A. Nelson, Linear intercept technique for measuring grain size in two-phase polycrystalline ceramics, J. Am. Ceram. Soc. 55 (1972) 109.
[23] O. Guillon, I. Nettleship, Microstructural characterization of alumina films during constrained sintering, J. Am. Ceram. Soc. 93 (3) (2010) 627–629.
[24] X. Wang, J.- Kim, A. Atkinson, Constrained sintering of 8 mol% Y_2O_3 stabilised zirconia films, J. Eur. Ceram. Soc. 32 (16) (2012) 4121–4128.
[25] P.Z. Cai, D.J. Green, G.L. Messing, Constrained densification of alumina/zirconia hybrid laminates, II: viscoelastic stress computation., J. Am. Ceram. Soc. 80 (8) (1997) 1940–1948.
[26] T. Rasp, C. Jamin, A. Wonisch, T. Kraft, O. Guillon, Shape distortion and delamination during constrained sintering of ceramic stripes: discrete element simulations and experiments, J. Am. Ceram. Soc. 95 (2) (2012) 586–592.